DOI 10.24425/aee.2024.150897

Analysis and estimation of power losses in high-power, high-frequency transformers for isolated DC/DC converters

PIOTR GRZEJSZCZAK ✉, ROMAN BARLIK, KORNEL WOLSKI

Institute of Control and Industrial Electronics, Warsaw University of Technology
Koszykowa 75, 00-662 Warszawa, Poland
e-mail: {✉ piotr.grzejszczak/roman.barlik/kornel.wolski}@pw.edu.pl

(Received: 28.02.2024, revised: 23.08.2024)

Abstract: The paper presents an in-depth analysis of the power losses in the windings and the cores of two different transformers as applied to a phase-shifted full bridge (PSFB) converter at the power level of 20–25 kW and the switching frequency of 50 kHz. The main difference in the construction of the considered devices was the method of winding realization as well as the shape and material of the cores. The influence of the winding geometry on the conduction losses was analyzed, and the losses in the cores were analytically estimated, taking into account the operating conditions of these elements in the full-bridge system with phase-shift modulation. Original resistive models of windings made of cooper sheets are presented. The obtained results were verified by experimental tests carried out in an isolated full-bridge DC/DC converter.

Key words: high-frequency power transformer, isolated DC/DC converter, power losses, proximity effect, skin effect

1. Introduction

The transformation of the electrical systems based on traditional utility power plants towards renewable energy sources and the dynamic development of electromobility that aims to provide widespread vehicle charger infrastructure are possible thanks to power electronics converters, primarily DC/DC converters. These devices should be capable of delivering sufficiently high-power levels (at least 20 kW) at high efficiency (at least 97%). In many cases, there is also the need to apply galvanic isolation between the input and the output of the converters [1, 2], which can

transfer the energy unidirectionally or in both directions. Figure 1 presents topologies of several of the most widely used DC/DC converters, which not only provide galvanic isolation but also enable matching between two sources at different DC voltage levels [3–6]. The critical component of this type of device is a high-frequency transformer, which provides galvanic isolation; however, at the same time requires the application of additional inverter (DC/AC) and rectifier (AC/DC) power conversion stages. The high-frequency transformer significantly impacts the converter's efficiency; therefore, the proper selection or design of this magnetic component determines the properties of the entire power electronic system.

This publication is devoted to analyzing power losses in high-frequency transformers applied in a 25 kW phase-shifted full bridge (PSFB) converter [7]. Construction of both the winding and the core structure, as well as other relevant aspects of transformer design, are discussed, taking into consideration the impact of the high harmonic content of voltage and current that occurs in topologies such as those shown in Fig. 1. The methods related to power loss estimation are well known and have already been described in literature related to high-frequency transformers, e.g. [8–13]. However, the discussed laboratory results are often limited to low power prototype. There is a distinct lack of application-oriented publications that would present power loss analyses in sufficient detail, as related to the current need for implementing transformers at increased switching frequencies in the case of high-efficiency DC/DC converters at power levels above 20 kW. This article presents, as follows: the subject of the research, including the structure of the cores and windings of the two analyzed transformers, calculation of the resistance of the primary and secondary windings for direct current and alternating current at a switching frequency of 50 kHz, calculation of power losses dissipated in the cores and windings of the transformers for specified operating points of the transformers, measurements of power losses in the analyzed transformers operating in the PSFB converter.

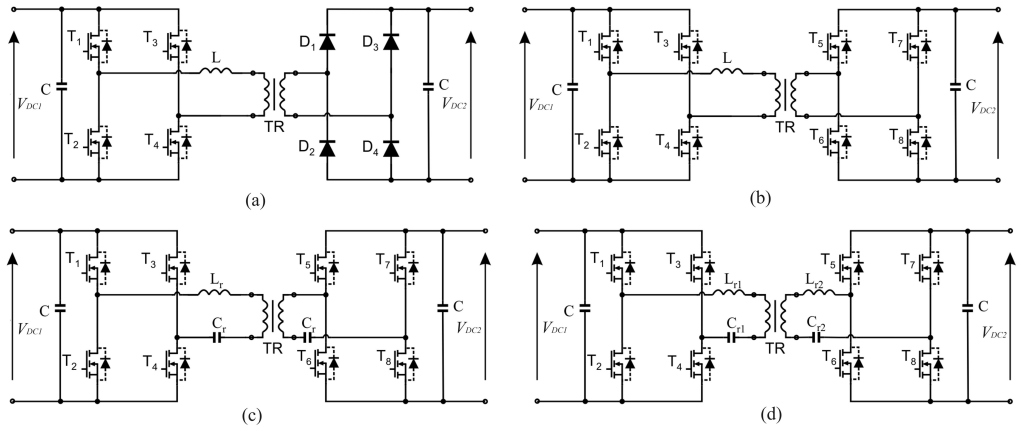

Fig. 1. The most prevalent DC/DC converter topologies with galvanic isolation: unidirectional full-bridge converter (a); bidirectional dual active bridge (DAB) (b); resonant DAB of the type CLLC (c) and CLLLC (d)

2. Parameters and construction details of the tested transformers

In the case of high-frequency transformers designed for high-power applications, there is a requirement to use windings with sufficiently large cross-section areas and, consequently, large window dimensions of the magnetic cores [14, 15]. The aim should be to maximize the window utilization while balancing the winding losses P_{Cu} and the core losses P_{Fe} [7] to minimize their sum $P_{Fe} + P_{Cu}$. The high frequency of the voltage and magnetic flux necessitates the usage of special magnetic core materials (usually ferrite) and wires that can assure the minimization of core losses and winding losses, respectively. The most common are high-frequency transformers implemented on toroidal cores or E-shaped cores of classic or planar structures. The windings are usually realized using thin copper sheets, printed circuit boards with copper tracks acting as windings, arranged in one plane (less often in a three-dimensional, helical version), or the so-called litz wires composed of many thin, mutually insulated strands.

Two types of transformers were selected for further analysis: one with a planar core structure placed inside of an air-cooled heat sink (Fig. 2(a)) and the other with a core composed of several E-type shapes (Fig. 2(b)). The windings were made of copper sheets and litz wires, respectively.

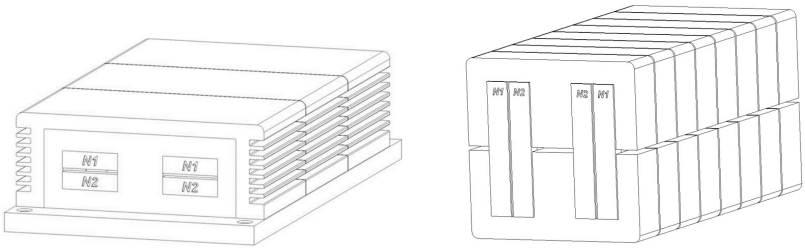

(a) (b)

Fig. 2. Sketches of the 25 kW transformers with: planar ferrite core structure (a) and a core arrangement of typical E-type ferrite shapes (b)

The main parameters for the considered transformers are presented in Table 1.

Table 1. Parameters of the 25 kW high-frequency transformers

Parameter	Symbol	Unit	Planar core	E-type core
Turn ratio	N_1/N_2	–	10/9	10/9
DC resistance of the primary winding	$R_{DC(N1)}$	mΩ	3.45	10.8
DC resistance of the secondary winding	$R_{DC(N2)}$	mΩ	2.85	10.6
Leakage inductance	L_r	μH	1.41	4.5
Magnetizing inductance	L_m	μH	672	2050
Winding type	–	–	0.5 mm copper sheets	Litz wire

3. Power loss estimation

3.1. The planar transformer

The analysis of the structure of the planar transformer allowed the identification of the parameters of its magnetic core and the method of construction of the windings (Fig. 3).

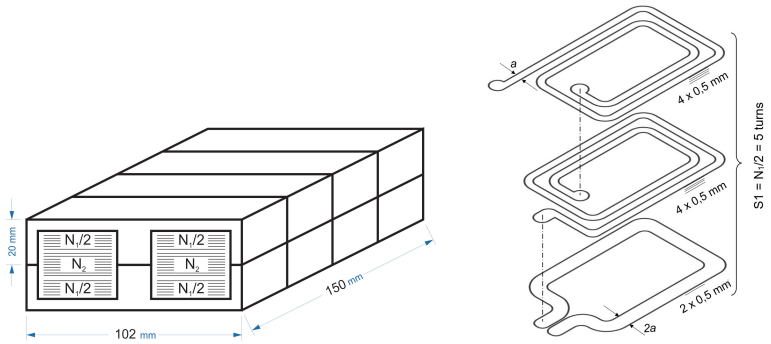

(a) (b)

Fig. 3. Sketch of the analyzed planar transformer (a) and the implementation of winding layers made of copper sheet with a thickness of 0.5 mm and a width of $a = 11$ mm (b)

Since with the adopted winding implementation, short circuits may occur between individual sheet copper plates constituting the given windings, to determine the resistance of the windings for direct current, this resistance was measured, and calculations were conducted for each plate (assuming resistivity $\rho = 1.7 \cdot 10^{-8}$ Ω·m).

Based on the identified configuration of windings made of copper sheet plates with a thickness of $h = 0.5$ mm, a diagram was compiled of the distribution of the magnetomotive force F along the edge of the core window (Fig. 4).

Based on the magnetomotive force diagram, the geometric configuration of the windings was determined as defined by the winding sections S1, S2, and S3 and the number of layers in these sections for the primary side $m_{s1} = m_{s3} = 3$ and secondary side $m_{s2} = 4$. These parameters made it possible to determine the K_R coefficients that define the increase of the winding resistance for alternating current ($R_{ac(N1)}$, $R_{ac(N2)}$) in relation to the resistance of these windings for direct current ($R_{dc(N1)}$, $R_{dc(N2)}$). The graphs presented in Fig. 5 were used, obtained based on Dowell's relationship (1) of the form ([9–12]):

$$R_{ac(j)} = R_{dc(j)} y \left[\frac{\sinh(2y) + \sin(2y)}{\cosh(2y) - \cos(2y)} + \frac{2}{3}\left(m_s^2 - 1\right) \frac{\sinh(y) - \sin(y)}{\cosh(y) + \cos(y)} \right] = R_{dc(j)} K_{R(j)}, \quad (1)$$

where: $R_{dc(j)}$ is the DC resistance of the j-th winding section; $K_{R(j)}$ is the resistance increase coefficient of the j-th section with the flow of AC current at the switching frequency f_s; m_s is the number of layers in the j-th winding section; y is the layer thickness ratio in relation to the skin depth ($\delta = 0.311$ mm at 50 kHz and the temperature of 20°C).

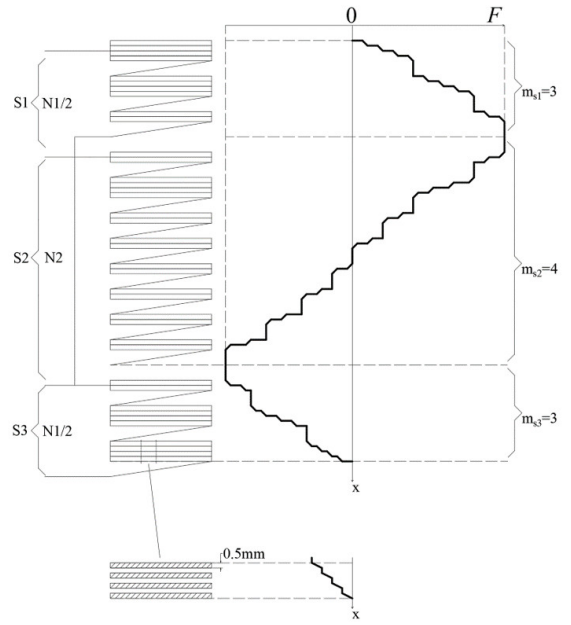

Fig. 4. The magnetomotive force diagram of the planar transformer

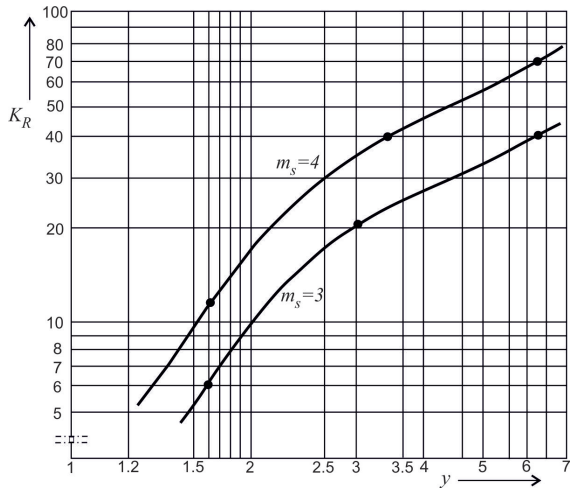

Fig. 5. AC loss factor K_{R} for windings with the number of layers equal to 3 and 4 as a function of the layer thickness ratio y

Equivalent diagrams of windings N_1 and N_2 made of copper plates and the results of calculations regarding the coefficients $K_{\mathrm{R}(j)}$ and the resistance values $R_{\mathrm{ac(N1)}}$ and $R_{\mathrm{ac(N2)}}$ are presented in Figs. 6 and 7, with $R_{\mathrm{ac(N1)}} = K_{\mathrm{R1}} \cdot R_{\mathrm{dc(N1)}}$ and $R_{\mathrm{ac(N2)}} = K_{\mathrm{R2}} \cdot R_{\mathrm{dc(N2)}}$.

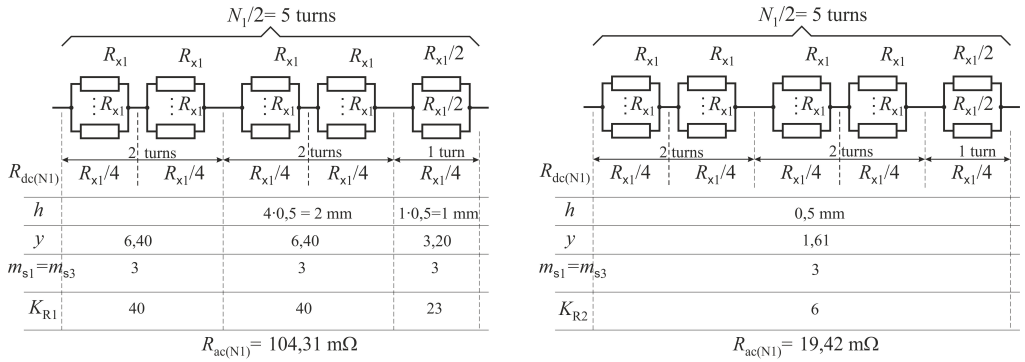

Fig. 6. Equivalent diagram of the primary-side winding resistance of the planar transformer: mutually insulated winding plates (R_{x1} = 1.294 mΩ, $R_{dc(N1)}$ = 3.42 mΩ, $R_{ac(N1)} = K_{R1} \cdot R_{dc(N1)}$ = 19.42 mΩ) (a); non-insulated winding plates (R_{x1} = 1.38 mΩ, $R_{dc(N1)}$ = 3.45 mΩ, $R_{ac(N1)} = K_{R2} \cdot R_{dc(N1)}$ = 104.31 mΩ) (b)

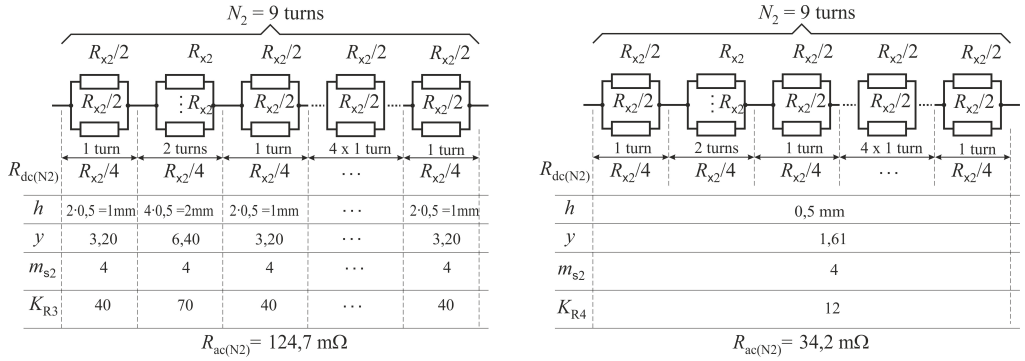

Fig. 7. Equivalent diagram of the secondary-side winding resistance of the planar transformer: mutually insulated winding plates (R_{x2} = 1.294 mΩ, $R_{dc(N2)}$ = 2.592 mΩ, $R_{ac(N2)} = K_{R3} \cdot R_{dc(N2)}$ = 31 mΩ) (a); non-insulated winding plates (R_{x2} = 1.425 mΩ, $R_{dc(N2)}$ = 2.85 mΩ, $R_{ac(N2)} = K_{R4} \cdot R_{dc(N2)}$ = 124.7 mΩ) (b)

A summary of the results of calculations and measurements of the resistance values of the primary and secondary windings for DC and AC is provided in Table 2. The division into windings with insulated plates (windings made correctly) and non-insulated plates (windings made incorrectly) is introduced. Resistance measurements were performed with a precision impedance analyzer LCR-8101G, the DC resistance measurement accuracy of which is 0.1%.

Based on the AC winding resistance at the frequency of 50 kHz and the RMS values of currents in the primary $I_{1(RMS)}$ = 32 A and the secondary winding $I_{2(RMS)}$ = 35.6 A, corresponding to the converter load of P_o = 16 kW, the power losses in both transformer windings (Table 3) were calculated. Similar calculations were performed for the converter power level of 20 kW. Due to the lack of clear information about mutual galvanic insulation between the plates from which the windings are made, calculations were carried out for insulated and non-insulated sheet variants. The calculations assume that in the case of triangular or trapezoidal current waveform shapes, there is no

need to determine power losses in the windings caused by individual harmonic components of the currents. As shown in [12], without committing an error greater than 6%, it is enough to consider the RMS values of such distorted currents and the fundamental frequency of these currents.

Table 2. Primary-side (N1) and secondary-side (N2) winding resistance values of the planar transformer

Parameter	Symbol	Unit	Comment	Primary side	Secondary side
DC resistance of the winding (at 20°C)	$R_{dc(N1)}$ $R_{dc(N2)}$	mΩ	Measured	2.85	3.45
	$R_{dc(N1)}$ $R_{dc(N2)}$		Calculated	3.24	2.59
AC resistance of the winding at 50 kHz – insulated plates	$R_{ac(N1)}$ $R_{ac(N2)}$		$R_{dc(N1)}$, $R_{dc(N2)}$ measured	17.10	41.40
	$R_{ac(N1)}$ $R_{ac(N2)}$		$R_{dc(N1)}$, $R_{dc(N2)}$ calculated	19.42	31.00
AC resistance of the winding at 50 kHz – non-insulated plates	$R_{ac(N1)}$ $R_{ac(N2)}$		$R_{dc(N1)}$, $R_{dc(N2)}$ measured	104.31	150.94
	$R_{ac(N1)}$ $R_{ac(N2)}$		$R_{dc(N1)}$, $R_{dc(N2)}$ calculated	118.54	113.30

Table 3. Power losses in the windings of the primary side (N1) and the secondary side (N2) of the planar transformer

Parameter	Symbol	Unit	Comment	Primary side	Secondary side
Winding losses at 16 kW and 50 kHz – insulated plates	P_{wind}	W	$R_{dc(N1)}$, $R_{dc(N2)}$measured	17.5	52.5
			$R_{dc(N1)}$, $R_{dc(N2)}$ calculated	19.9	39.3
Winding losses at 16 kW and 50 kHz – non-insulated plates			$R_{dc(N1)}$, $R_{dc(N2)}$ measured	106.8	191.3
			$R_{dc(N1)}$, $R_{dc(N2)}$ calculated	121.1	143.6
Winding losses at 20 kW and 50 kHz – insulated plates			$R_{dc(N1)}$, $R_{dc(N2)}$ measured	34.6	103.5
			$R_{dc(N1)}$, $R_{dc(N2)}$ calculated	39.3	77.5
Winding losses at 20 kW and 50 kHz – non-insulated plates			$R_{dc(N1)}$, $R_{dc(N2)}$ measured	211.2	377.4
			$R_{dc(N1)}$, $R_{dc(N2)}$ calculated	240.1	283.3

When analytically determining power losses in the core of the planar transformer, where magnetic core halves of the type 0R49938EC [16] were applied, loss characteristics of dependence on the peak value of magnetic flux density (Fig. 8) and its frequency were used.

For the peak flux density value B_m = 143 mT (calculated based on the rectangular primary winding voltage V_m = 600 V and the core cross-section area S_{Fe} = 2100 mm^2), the loss density is $p_{Fe} \approx 50$ mW/cm^3. This is obtained based on the Steinmetz equation and the core loss vs flux density characteristic shown in [16]. This approach takes into considerations all the relevant high-frequency flux components in the core. Considering the core volume V_{Fe} = 324.72 cm^3, the power losses in the core $P_{Fe} = p_{Fe} \cdot V_{Fe}$ = 16.2 W are obtained. This value is relatively small, indicating that the core is oversized for the assumed transformer operating point.

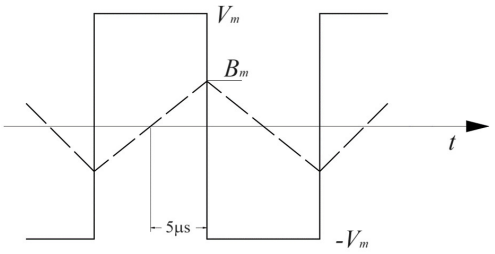

Fig. 8. Waveforms of the magnetic flux density and the primary-side voltage of the planar transformer at f_s = 50 kHz (B_m, V_m – peak flux density and maximum voltage value, respectively)

3.2. E-type core transformer

A sketch of the transformer is shown in Fig. 9. The windings were made of 1050 × 0.1 mm litz wire. The number of turns of the primary and secondary windings was N_1 = 10 and N_2 = 9, respectively, with the lengths of the wire used l_{N1} = 4.4 m and l_{N2} = 3.96 m. Considering copper resistivity ρ = 0.0178 Ω·m (at the temperature of 20°C), the calculated resistance values of the windings are $R_1 \approx 10$ mΩ and $R_2 \approx 9$ mΩ, respectively. Taking into account the inaccuracy of estimating the lengths of the windings, the resistance of both windings was also measured, obtaining the following results: $R_{1(dc)} \approx 10.6$ mΩ and $R_{2(dc)} \approx 10.8$ mΩ, respectively. Due to the negligible skin and proximity effects in the litz wire, for the calculations of power losses in the windings it was assumed that their resistance values at the frequency of 50 kHz are equal to the resistance values at DC ($R_{ac} \approx R_{dc}$). Power losses in the windings for currents $I_{1(RMS)}$ = 32 A and $I_{2(RMS)}$ = 35.6 A, corresponding to the converter output power P_o = 16 kW, are ΔP_{N1} = 10.85 W and ΔP_{N2} = 13.69 W, respectively.

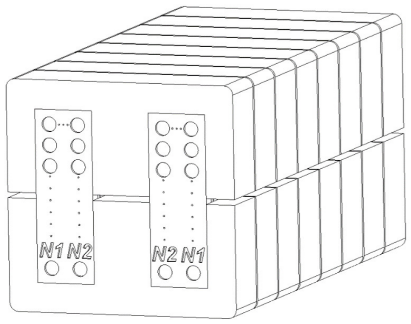

Fig. 9. The sketch of the transformer based on E-shaped core halves and litz wire

The transformer core was constructed using eight pairs of the E80/38/20 core halves made of 3C92 ferrite material [17]. Power losses in the core were determined using the Steinmetz relationship of the form

$$p_{Fe} = k f^{\alpha} B_m^{\beta} \left[\frac{W}{m^3}\right], \tag{2}$$

where $B_m \approx 90$ mT is the peak value of the alternating (triangular) core flux density waveform, determined on the basis of the rectangular primary winding voltage U of ±600 V, frequency f of 50 kHz, and the core cross-section area S_{Fe} = 3200 mm^2. The Steinmetz coefficients that appear

in the given relationship are: $k = 2.37$; $\alpha = 1.46$; $\beta = 2.75$, as obtained based on the core loss density characteristics shown in [18]. For such determined sizes and parameters, the loss density of the ferrite core is $p_{\mathrm{Fe}} = 22.9$ mW/cm^3, while the power losses in the core (assuming volume $V_{\mathrm{Fe}} = 614.4$ cm^3) can be calculated as follows:

$$P_{\mathrm{Fe}} = p_{\mathrm{Fe}} V_{\mathrm{Fe}} = 14.07 \text{ W}. \tag{3}$$

Also, in the case of this transformer, a small value of these losses indicates oversizing of the core. It should be added, however, that this was intentional and resulted from the purpose of the transformer, which is to be placed in a device with limited possibility of using forced cooling. With such limitations, the core serves the role of a heat sink that must dissipate not only the heat generated in the core but, above all, that resulting from power losses generated in the windings.

4. Simulation study

In order to estimate total power losses in the entire converter that is composed of two bridges (single-phase voltage inverter with SiC MOSFET transistors and a Graetz bridge with SiC Schottky diodes - Fig. 10), power losses in semiconductor elements were determined based on a simulation model implemented in PLECS. For the system operating point corresponding to the output power $P_{\mathrm{o}} = 16$ kW, the values of power losses in particular test system components are presented in Table 4.

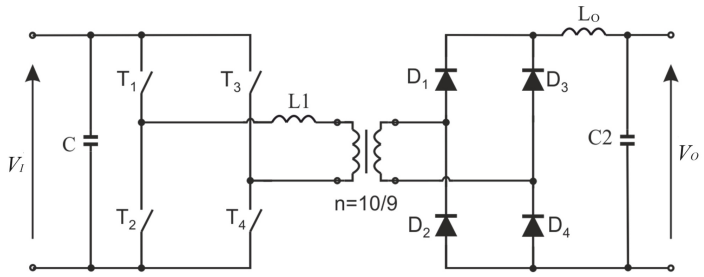

Fig. 10. The converter topology assumed for the simulation and the experimental studies

Based on the simulation results, crucial parameters related to current and voltage waveforms were obtained. The switch-off current and voltage values as well as the RMS values of the transistor currents allowed to estimate the MOSFET losses $\Delta P_{\mathrm{T,sw}}$ and $\Delta P_{\mathrm{T,cond}}$, using the method described in [7]. It should be noted that, due to the lack of relevant data, a linear dependence of the gate resistance on the value of turn-off energy was assumed. For the SiC Schottky diodes the switching losses were assumed to be negligible and only the RMS and average diode current values were required to calculate the loss value ΔP_D. As for the inductors, the simulation waveforms allowed to estimate the core losses based on the Steinmetz Eq. (2) and the RMS current values were used to obtain the winding losses, which resulted in the total inductor losses for the coupling inductor and the output inductor (ΔP_{Ll} and ΔP_{Lo}). Note that because of different values of transformer leakage and magnetizing inductance, L_{r} and L_{m} (Table 1), the waveform shapes in case of each transformer are different.

Table 4. Simulation results at the power level of 16 kW

Parameter	Symbol	Unit	Planar core		E-type core	
Gate resistance	R_g	Ω	2.5	10	2.5	10
Switching losses in the MOSFETs	$\Delta P_{T,sw}$	W	25	102	27	106
Conduction losses in the MOSFETs	$\Delta P_{T,cond}$		47		54	
Conduction losses in the diodes	ΔP_D		104		117	
Total semiconductor losses	$\Delta P_{tot,semi}$		176	253	197	277
Losses in the coupling inductor L_l	ΔP_{Ll}		14		14	
Losses in the output inductor L_o	ΔP_{Lo}		10		11	

5. Experimental tests

The obtained results of calculations and simulation tests were verified by tests of a laboratory model of the converter, conducted using the topology shown in Fig. 10. Figure 11 shows a photos of the experimental setup capable of investigating voltage and current waveforms (Fig. 12) of the primary winding and the determining the total power losses occurring in the converter.

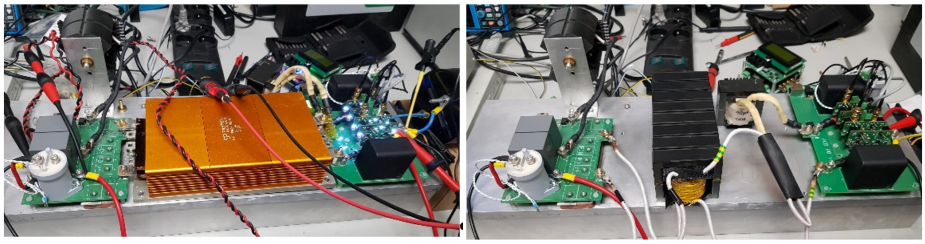

Fig. 11. Photographs of the experimental setup for the DC/DC converter with the planar transformer (a) and with the E-core-based transformer (b)

Total transformer losses ΔP_{TR} can be expressed using two alternative Formulas: (4) and (5).

$$\Delta P_{TR} = \Delta P_{N1} + \Delta P_{N2} + \Delta P_{Fe}, \tag{4}$$

where: ΔP_{N1} is the power loss in the primary winding of the transformer, ΔP_{N2} is the loss in the secondary winding of the transformer, ΔP_{Fe} is the core loss.

$$\Delta P_{TR} = P_i - P_o - \Delta P_{Ll} - \Delta P_{Lo} - \Delta P_{tot,semi}, \tag{5}$$

where: P_i is the converter input power, P_o is the output power, ΔP_{Ll} is the power loss in the inductor L_l, ΔP_{Lo} is the loss in the inductor L_o, $\Delta P_{tot,semi}$ is the total semiconductor loss.

Based on the calculations, simulations, and measurements, the following results were obtained:

a) windings made of insulated sheets:
   – for the AC winding resistance values $R_{ac(N1)}$ and $R_{ac(N2)}$ determined based on the calculated DC winding resistance values $R_{dc(N1),calc}$ and $R_{dc(N2),calc}$:
   $\Delta P_{TR,calc} = 353$ W,

– for the AC winding resistance values $R_{ac(N1)}$ and $R_{ac(N2)}$ determined based on the measured DC winding resistance values $R_{dc(N1),meas}$ and $R_{dc(N2),meas}$:
$\Delta P_{TR,meas} = 357$ W,

b) windings made of non-insulated sheets:
– for the AC winding resistance values $R_{ac(N1)}$ and $R_{ac(N2)}$ determined based on the calculated DC winding resistance values $R_{dc(N1),calc}$ and $R_{dc(N2),calc}$:
$\Delta P_{TR,calc} = 557$ W,
– for the AC winding resistance values $R_{ac(N1)}$ and $R_{ac(N2)}$ determined based on the measured DC winding resistance values $R_{dc(N1),meas}$ and $R_{dc(N2),meas}$:
$\Delta P_{TR,meas} = 581$ W,

c) transformer power losses obtained experimentally, based on (5):
$\Delta P_{TR,exp} = 561$ W.

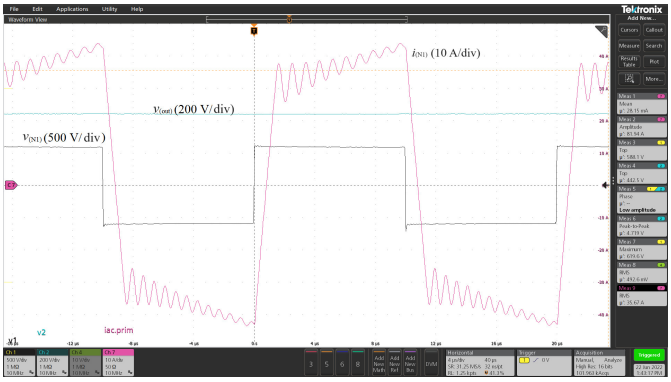

(a)

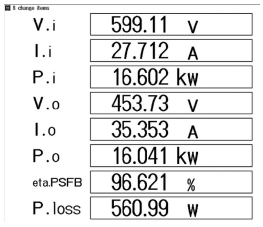

(b)

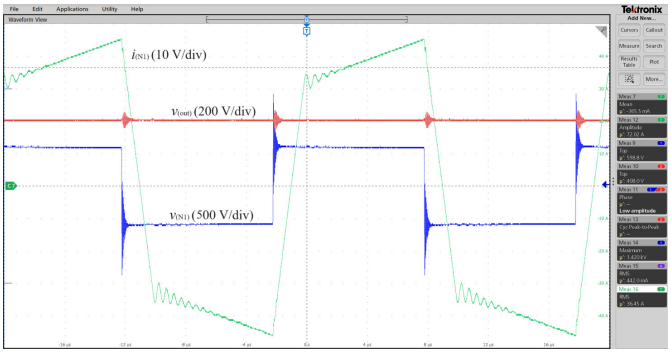

(c)

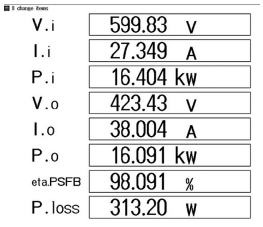

(d)

Fig. 12. Waveforms of the voltage ($v_{(N1)}$) and current ($i_{(N1)}$) of the primary-side winding of the transformer, the output voltage ($v_{(out)}$) at the power level of 16 kW ($I_{1(RMS)} = 32$ A; $I_{2(RMS)} = 35.6$ A), and the power analyzer results for: the setup with the planar transformer (a), (b) and with the E-core-based transformer (c), (d)

The calculation and measurement results for the planar transformer and the transformer based on E-type cores are presented in Table 5.

Table 5. Calculation and experimental results at the output power level of 16 kW

Derivation method	**Symbol**	**Planar core**				**E-type core**	
		Insulated Cu sheets		Non-insulated Cu sheets			
		Total power loss	Error	Total power loss	Error	Total power loss	Error
Analytical meas	P_{loss}	357 W	–36%	581 W	4%	341 W	9%
Analytical calc		353 W	–37%	557 W	–1%	348 W	11%
Experimental		561 W				313 W	

The highest error of approximately 40% resulted for the case of the planar transformer under the assumption that the windings are made of insulated Cu sheets. However, the obtained results indicate that this hypothesis was not valid. In fact, it should be assumed that the windings are made of non-insulated sheets for which the error between measured and calculated losses does not exceed 5%.

Figure 13 shows the measurement results of total power losses in the PSFB converter depending on the output power. Measurements of the converter's power losses were performed using a precise Yokogawa WT1800 power analyzer, through the difference in power in the output and input DC circuits. Accuracy for DC circuits is ±(0.05% of reading +0.1% of range) for voltage and ±(0.05% of reading +0.1% of range) for current, and therefore ±(0.1% of reading +0.1% of range) for power measurements. Analyzing the obtained results, an increasingly significant impact of power losses in the transformer windings made of copper sheets is visible compared to power losses in the litz wire, in which the unfavorable high-frequency effects are negligible.

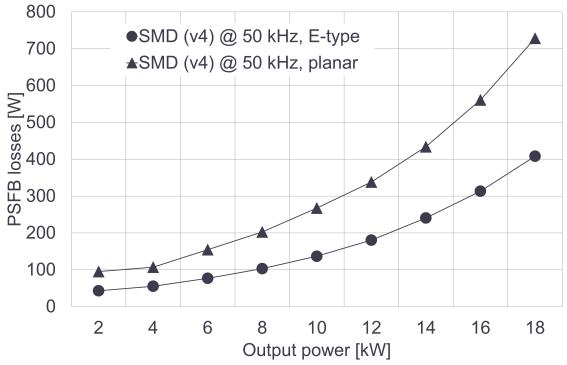

Fig. 13. Characteristics of the total power losses of the converter as a function of the output power, measured with Yokogawa WT1800 power analyzer in the variants with a planar transformer and a transformer with E-type cores

6. Conclusions

The presented calculation-based and experimental analysis of power losses covers various construction variants of the copper sheets and litz wire windings. Careful considerations have shown that the most significant convergence of analytical calculations and experimental measurement results occurs with windings made of non-insulated copper sheets. It can be concluded that these windings were made with a particular defect, whereby instead of a winding in the form of a thin (0.5 mm) sheet of copper, there are sections of winding that have a thickness corresponding to four times the thickness of the copper sheet used (2 mm). With such a large thickness, the influence of the skin effect and the proximity effect is highlighted, increasing K_{R1} and K_{R2} coefficients and, therefore, the resistance to alternating current at 50 kHz. The proposed method of determining the winding resistance for direct current and for a frequency of 50 kHz allowed for a relatively accurate estimation of the total power losses of the transformer and a fully satisfactory convergence of the calculation results and power loss measurements. The differences do not exceed 11% for E-type and Litz wire transformer (Table 5).

Acknowledgements

The research was supported by The National Centre for Research and Development (NCBR) grant number MAZOWSZE/0111/19 „SIMES – Smart Integrated Modular Energy System for DC microgrids with renewable energy sources and energy storage".

References

[1] Wouters H., Martinez W., *Bidirectional Onboard Chargers for Electric Vehicles: State-of-the-Art and Future Trends*, IEEE Transactions on Power Electronics, vol. 39, no. 1, pp. 693–716 (2024), DOI: 10.1109/TPEL.2023.3319996.

[2] Santos N., Chaves M., Gamboa P., Cordeiro A., Santos N., Pinto S.F., *High Frequency Transformers for Solid-State Transformer Applications*, Applied Sciences, vol. 13, no. 12, pp. 7262 (2023), DOI: 10.3390/app13127262.

[3] Zhang X., Xiao F., Wang R., Kang W., Yang B., *Modeling and Design of High-Power Enhanced Leakage-Inductance-Integrated Medium-Frequency Transformers for DAB Converters*, Energies, vol. 15, no. 4, 1361 (2022), DOI: 10.3390/en15041361.

[4] Li Y., Wang R., Zhong L., Mao L., Sun C., Li X., Hu S., *Analysis and Design of a High-Frequency Isolated Dual-Transformer DC–DC Resonant Converter*, Electronics, vol. 12, no. 1, 103 (2023), DOI: 10.3390/electronics12010103.

[5] Saket M.A., Shafiei N., Ordonez M., *LLC Converters with Planar Transformers: Issues and Mitigation*, IEEE Transaction on Power Electronic, vol. 32, no. 6, pp. 4524–4542 (2017), DOI: 10.1109/TPEL.2016.2602360.

[6] Escudero M., Kutschak M.-A., Meneses D., Rodriguez N., Morales D.P., *A Practical Approach to the Design of a Highly Efficient PSFB DC–DC Converter for Server Applications*, Energies, vol. 12, no. 19, pp. 3723 (2019), DOI: 10.3390/en12193723.

[7] Wolski K., Grzejszczak P., Szymczak M., Barlik R., *Closed-Form Formulas for Automated Design of SiC-Based Phase-Shifted Full Bridge Converters in Charger Applications*, Energies, vol. 14, no. 17, 5380 (2021), DOI: 10.3390/en14175380.

[8] Yi Z., Sun K., Liu H., Zhang Q., *Modeling and Evaluation of Ferrite Eddy Losses in High-Frequency Transformers Based on Loss-Effective Conductivity Extraction*, IEEE Journal of Emerging and Selected Topics in Power Electronics, vol. 11, no. 6, pp. 5990–6004 (2023), DOI: 10.1109/JESTPE.2023.3314062.

[9] Bahmani M.A., Thiringer T., Ortega H., *An Accurate Pseudoempirical Model of Winding Loss Calculation in HF Foil and Round Conductors in Switchmode Magnetics*, IEEE Transactions on Power Electronics, vol. 29, no. 8, pp. 4231–4246 (2014), DOI: 10.1109/TPEL.2013.2292593.

[10] Dowell P.L., *Effects of eddy currents in transformer windings*, Proceedings of the Institution of Electrical Engineers, vol. 113, no. 8, pp. 1387–1394 (1966), DOI: 10.1049/piee.1966.0236.

[11] Petkov R., *Optimum design of a high-power, high-frequency transformer*, IEEE Transactions on Power Electronics, vol. 11, no. 1, pp. 33–42 (1996), DOI: 10.1109/63.484414.

[12] Barlik R., Nowak M., Grzejszczak P., Zdanowski M., *Analytical description of power losses in a transformer operating in the dual active bridge converter*, Bulletin of the Polish Academy of Sciences Technical Sciences, vol. 64, no. 3, pp. 561–574 (2016), DOI: 10.1515/bpasts-2016-0063.

[13] Barlik R., Nowak M., Grzejszczak P., Zdanowski M., *Estimation of power losses in a high-frequency planar transformer using a thermal camera*, Archives of Electrical Engineering, vol. 65, no. 3, pp. 613–627 (2016), DOI: 10.1515/aee-2016-0044.

[14] Guo Z., Yu R., Xu W., Feng X., Huang A., *Design and optimization of a 200-kW medium-frequency transformer for medium-voltage SiC PV inverters*, IEEE Transaction on Power Electronics, vol. 36, no. 9, pp. 10548–10560 (2021), DOI: 10.1109/TPEL.2021.3059879.

[15] Nabih A., Jin F., Gadelrab R., Lee F.C., Li Q., *Characterization and Mitigation of Dimensional Effects on Core Loss in High-Power High-Frequency Converters*, IEEE Transactions on Power Electronics, vol. 38, no. 11, pp. 14017–14036 (2023), DOI: 10.1109/TPEL.2023.3285633.

[16] www.mag-inc.com/Products/Ferrite-Cores/R-Material, accessed May 2024.

[17] www.ferroxcube.com/upload/media/product/file/Pr_ds/E80_38_20.pdf, accessed May 2024.

[18] https://ferroxcube.home.pl/prod/assets/3c92.pdf, accessed May 2024.